Research Paper

Non-invasive real-time imaging of reactive oxygen species (ROS) using auto-fluorescence multispectral imaging technique: A novel tool for redox biology

Abbas Habibalahi[a],[*],[1], Mahdieh Dashtbani Moghari[b],[1], Jared M. Campbell[a], Ayad G. Anwer[a], Saabah B. Mahbub[a], Martin Gosnell[c], Sonia Saad[d], Carol Pollock[d], Ewa M. Goldys[a]

[a] ARC Centre of Excellence Centre for Nanoscale Biophotonics, University of New South Wales, Kensington, 2052, NSW, Australia
[b] School of Biomedical Engineering, Faculty of Engineering, Darlington Campus, The University of Sydney, NSW, 2006, Australia
[c] Quantitative Pty Ltd, ABN 17 165 684 186, Australia
[d] Kolling Institute of Medical Research, University of Sydney, Camperdown, 2006, NSW, Australia

A B S T R A C T

Detecting reactive oxygen species (ROS) that play a critical role as redox modulators and signalling molecules in biological systems currently requires invasive methods such as ROS -specific indicators for imaging and quantification. We developed a non-invasive, real-time, label-free imaging technique for assessing the level of ROS in live cells and thawed cryopreserved tissues that is compatible with *in-vivo* imaging. The technique is based on autofluorescence multispectral imaging (AFMI) carried out in an adapted fluorescence microscope with an expanded number of spectral channels spanning specific excitation (365 nm–495 nm) and emission (420 nm–700 nm) wavelength ranges. We established a strong quantitative correlation between the spectral information obtained from AFMI and the level of ROS obtained from CellROX staining. The results were obtained in several cell types (HeLa, PANC1 and mesenchymal stem cells) and in live kidney tissue. Additioanly, two spectral regimes were considered: with and without UV excitation (wavelengths > 400 nm); the latter being suitable for UV-sensitive systems such as the eye. Data were analyzed by linear regression combined with an optimization method of swarm intelligence. This allowed the calibration of AFMI signals to the level of ROS with excellent correlation (R = 0.84, p = 0.00) in the entire spectral range and very good correlation (R = 0.78, p = 0.00) in the limited, UV-free spectral range. We also developed a strong classifier which allowed us to distinguish moderate and high levels of ROS in these two regimes (AUC = 0.91 in the entire spectral range and AUC = 0.78 for UV-free imaging). These results indicate that ROS in cells and tissues can be imaged non-invasively, which opens the way to future clinical applications in conditions where reactive oxygen species are known to contribute to progressive disease such as in ophthalmology, diabetes, kidney disease, cancer and neurodegenerative diseases.

1. Introduction

Accurate reactive oxygen species (ROS) quantification and characterization plays an important role in the investigation of metabolism [1,2], inflammatory responses [3–5], the pathogenesis of the disease [6,7], treatment monitoring [8–11] and potentially provides prognostic information [12–15]. Currently, standard ROS measurement uses various molecular indicators such as dichlorofluorescein, a fluorescent probe that reacts intracellularly with peroxidase, or CellROX, a fluorogenic probe for measuring oxidative stress in live cells and tissue [16–18]. However, due to challenges with administration and potential toxicity molecular ROS probes may not be suitable for in-vivo use [16,19]. To overcome these limitations an imaging technique which can measure ROS levels directly, without any staining, in clinical and research environments, is highly desirable.

In this study, we employed autofluorescence multispectral imaging (AFMI) [20,21] to non-invasively characterize ROS levels. The

autofluorescence emission in cells or tissues originates from endogenous fluorophores including collagen, elastin, tryptophan and reduced nicotinamide adenine dinucleotide (phosphate) (NAD(P)H), flavins [21–23]. The autofluorescence emission of some of these, most notably NAD(P)H, depends on its oxidation state. NAD(P)H is fluorescent wheras NAD+ is not, and the relative balance of these two depends on the level of ROS [24,25]. This allows the status of cellular, mitochondrial or cytosolic ROS to be non-invasively evaluated and monitored [26].

AFMI is a new technology that uses an adapted fluorescence microscope which provides light excitation in several narrow (+/- 5 nm) wavelength ranges and collects the native fluorescence emission of the sample, also at defined wavelength ranges [20,21]. Each excitation /emission wavelength band combination forms a specific spectral channel and we used a number of such channels (here 18) to collect detailed spectral image information from cells and tissue. Following AFMI, the slide-mounted cells and tissue were stained using CellROX

and imaged again to establish the reference ROS values. These were matched with the corresponding AFMI data in each individual cell or tissue section separately.

Non-invasive evaluation of ROS in real-time was achieved by calibrating the cellular AFMI data against the ROS data from CellROX, on a single-cell level. This calibration was based on selected color features extracted from the single-cell AFMI images and the corresponding CellROX images. The data sets were then used to develop classifiers, with a threshold based on the median of CellROX values, allowing the non-invasive determination of whether the ROS level in cells and tissues was moderate or elevated. We have also developed a UV-free version of the AFMI vs ROS (CellROX) calibration and a related UV-free classifier where the UV channels with excitation wavelengths of less than 400 nm were avoided; this is relevant for UV-sensitive applications such as in reproductive medicine and ophthalmology. Taken together these results represent a novel methodology that allows objective, non-invasively determination of ROS levels related to oxidative metabolism or redox dysregulation in cells and tissues from multispectral images using automated technology.

2. Methods

2.1. Sample preparation and ROS stimulation

In this study we investigated neoplastic cells (HeLa and PANC1), human bone marrow derived mesenchymal stem cells (MSC) (isolated as described previously [27,28]) and cryopreserved whole kidney tissue sections obtained from 13 week old Balb/c mice, which were exposed to either air or smoke in utero, as we have previously demonstrated that they express increased levels of ROS [29]. Full details of cell culture and ethics approvals are included in Supplementary Material note 1. To stimulate ROS accumulation, cells were exposed to 30μM menadione (Sigma) in the culture media for 0, 30, 60, 90 and 120 min. For imaging, cells were plated onto 35mm ibiTreat coverslip bottomed dishes with 500μm grids (Ibidi).

2.2. Autofluorescence multispectral imaging (AFMI)

The (AFMI) system used in this study is based on an adapted IX83 Olympus microscope as previously reported [22,30,31]. It provides narrow excitation wavelength ranges ($\pm$5nm) from high power LEDs and several filter cubes to produce defined spectral regions, which span the excitation (340 nm–510 nm) and emission (420 nm–650 nm) wavelength ranges. In total, 18 distinct spectral channels ($N_{ch} = 18$) are available and the samples are imaged in all these channels (examples of spectral channles are shown in Fig. 1(c,d)). These channels cover the spectrum of several fluorophores notably NAD(P)H and flavins, whose concentrations depend on the cellular redox conditions. The spectral details of the channels are shown in Supplementary Table 1. The system also takes differential contrast microscopy (DIC) images. A CCD camera with a high quantum efficiency (Andor IXON 885 EMCCD, Andor Technology Ltd., UK) was used to acquire the fluorescence images in the spectral channels. The images were captured at 40 × magnification (an example of MSC DIC image is shown in Fig. 1(a)).We imaged in the order of 100 cells from each cell type and about 70 tissue regions from the kidney tissue (~500um^2). The channel images were prepared for subsequent quantitative analysis. Image preparation is a multistep procedure that minimizes sources of errors such as Poisson's noise, dead or saturated pixels, background fluorescence and the illumination curvature [32]. These artifacts were treated as previously reported [21,33].

2.3. CellROX and nuclear staining

Following AFMI imaging, cell/tissue samples were stained with CellROX Deep Red (Thermo Fisher). CellROX Deep Red is a cell-permeant dye which stains the cytoplasm. This probe detects superoxide anion and hydroxyl radicals [34]. To obtain the reference ROS values, CellROX was applied to cells/tissue on the slides for 30 min as per manufacturer's instructions, followed by imaging on an Olympus FV3000 confocal microscope for hMSC cell lines and kidney tissue, or a Leica FLUOTAR340 for the cancer cell lines (an example CellROX image is shown in Fig. 1(b)). Nuclear counter-staining was performed with Hoechst 3(3342 (NucBlue, Thermo Fisher).

2.4. Image analysis

The cells and tissue regions were segmented manually, on the basis of their DIC images taken during AFMI imaging, and by using confocal CellROX images. Further, the average channel or CellROX values in the segmented cells or tissue regions were calculated. Autofluorescence feature vectors containing these average channel values (18 channels) and all ratio of average channel values (18 × 17 ratios) for each cell were obtained. The CellROX images were, similarly, segmented and the average cellular value of the CellROX signal (providing the reference ROS value) was found for each cell/tissue sector. Finally, the corresponding cells and tissue regions were identified in the AFMI and CellROX images. The ROS reference values were then appended to the 324-dimensional autofluorescence feature vectors (AFMI vectors) obtained from AFMI for all cells or tissue regions.

2.5. Calibration - relating AFMI to ROS reference values from CellROX

The aim of system calibration is to identify a small subset of AFMI features whose optimized linear combination is approximately proportional to the CellROX ROS values, for all individual cells, or tissue sectors. This is achieved by swarm intelligence [35] combined with the regression model [36,37]. The optimized linear combination of AFMI features (a "spectral variable") represents the cellular CellROX data in the "best" way, by numerically minimizing the sum of squared errors for all cells. The error is the difference between the average cellular CellROX values and the average values of that spectral variable for a particular cell or tissue region (see Supplementary Material note 2).

2.6. Non-invasive assessment of ROS by classification of AFMI data

To distinguish cells with high ROS levels from cells with moderate ROS levels, we developed the AFMI-based classification method. In this method cells and tissue regions were assigned to high or moderate ROS groups using the median cellular value of CellROX signal as a threshold.The cluster analysis was first applied to separate cell groups and further classifiers were employed to predict the pre-defined cell labels [38].

2.7. UV-free ROS calibration and classifiers

To develop the calibration and classifiers for UV-sensitive applications, the same analysis described in Sections 2.5 and 2.6 was conducted without AFMI channels with excitation at the UV range (excitation wavelengths from 400nm to 495nm).

3. Results and discussion

Linear regression combined with the method of swarm intelligence detected an approximately linear dependence between an optimized autofluorescence feature (spectral variable) and ROS levels determined by CellROX staining. This spectral variable was different for each sample and we did not find a significant similarity between spectral variables associated with different cell lines and tissue. The goodness of the calibration curves was statistically evaluated based on coefficient of determination (R) and associated p-values (Supplementary note 3 and supplementary table 2), which were found to range from 0.76
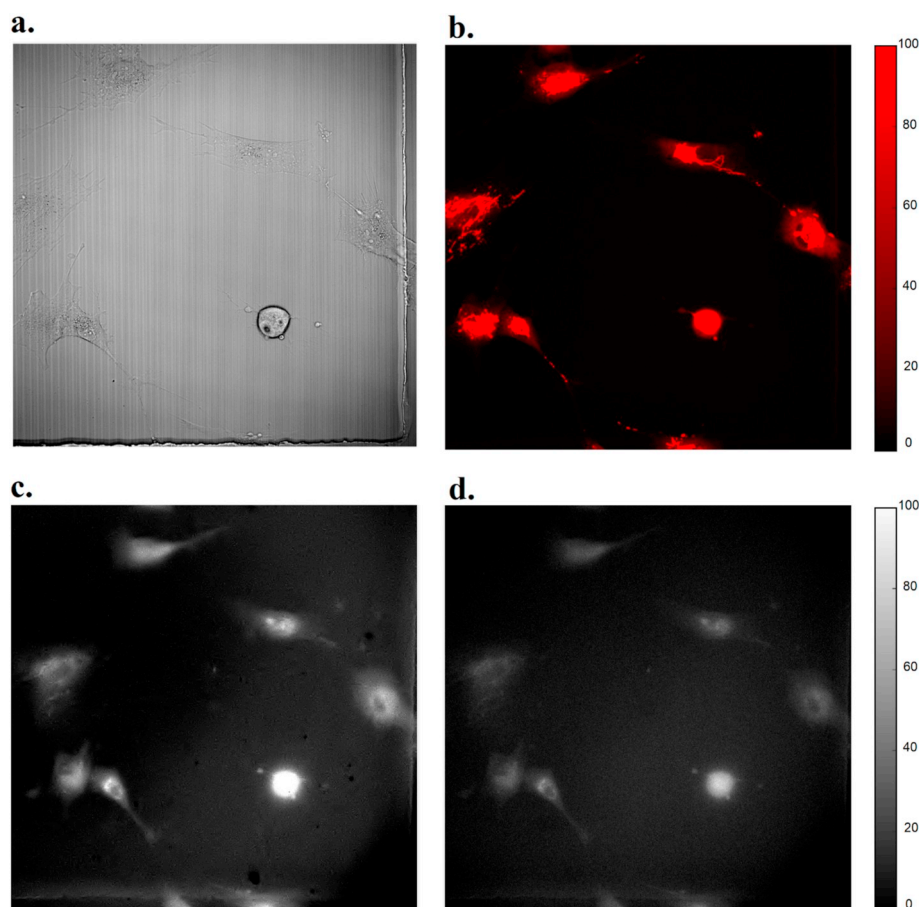
Fig. 1. (a) An example of MSC DIC image. (b) an example CellROX image. (c),(d) examples of spectral image channels 2 and 13, respectively.

(p = 0.00) to 0.92(p = 0.00) for the full excitation spectrum, and 0.74 (p = 0.00) to 0.87 (p = 0.00) (Fig. 2) for the UV-free spectrum (Supplementary Fig. 1). The lowest intracellular ROS concentration detectable by AFMI for HeLa/PANC1/MSC/kidney tissue is approximately 0.55 /0.50 /0.90 /1.2 of the average native fluorophore concentration, which is in the micromolar range [39–41].

We further developed classifiers to distinguish cells with a high level of ROS from those with a moderate level of ROS [38,42]. The same data and classification models developed here were used to evaluate the level of ROS in 3 different cell lines and kidney tissue. The classifiers were constructed using discrimination analysis to separate the cells with high-level ROS from cells with a moderate level [20](further details in supplementary note 4). Fig. 3 and Supplementary Figure 2 show the clusters formed by cells with high and moderate ROS level obtained using the entire excitation spectrum and UV-free excitation spectrum, respectively.

The receiver operating characteristic (ROC) graph was obtained to determine the performance of this classifier for each sample as shown in Fig. 4 [43]. Overall, the classifiers for different samples showed similar performance with average accuracies of 84% and 79% and AUCs of 0.91 and 0.87 for the entire excitation spectrum and UV-free excitation spectrum, respectively (see Supplementary Table 2 for further related statistics). The sensitivity of AFMI corresponding to true positive rate of the classifiers, averaged over all samples in Fig. 4 were found to be 89% and 83% for the entire excitation spectrum and for the UV-free excitation spectrum, respectively.

In this study, we demonstrate the use of a non-invasive auto-fluorescence multispectral imaging technique for the quantitative analysis of ROS-related spectral signatures of cells and tissue preserving spatial information. This technology is capable of measuring the value of ROS

with high accuracy and also classifying the cells into moderate and high levels of ROS. It does not perturb biology as it does not require cell labeling or any other interference, and it has the ability to assess cryopreserved and fixed tissue, reflecting the redox state of cells after fixation. We tested neoplastic cells (HeLa and PANC1), human bone marrow derived mesenchymal stem cells (MSC) and cryopreserved whole kidney tissue; however, this technique can be used for a range of different cell and tissue types.

Oxidative stress is a hallmark of multiple chronic diseases associated with older age such as diabetes, cardiovascular, renal, pulmonary, neurological and skeletal muscle disorders [44]. In addition, it is known to play a pivotal role in disease onset and development [45], such as the development and progression of diabetes complications both micro-vascular and macrovascular [46,47]. As such, our novel technique has great clinical application not only in disease detection but also in studying the underlying mechanisms and role of oxidative stress in disease onset and progression.

AFMI requires a fairly simple adaptation of a fluorescence microscope using low power LEDs (see Supplementary Material Table 1) [20]; this allows the extraction of informative spectral maps of cells and tissues which contain details on the biochemical composition of the sample which correlates with the level of ROS. This simplicity and low cost make AFMI easily translatable to the clinical setting. The immediate application of this study would be monitoring ROS state in embryology, reproductive medicine and ophthalmology.

4. Conclusions

In conclusion, we found that cellular autofluorescence imaging with spectral selectivity non-invasively determines the level of ROS in cells
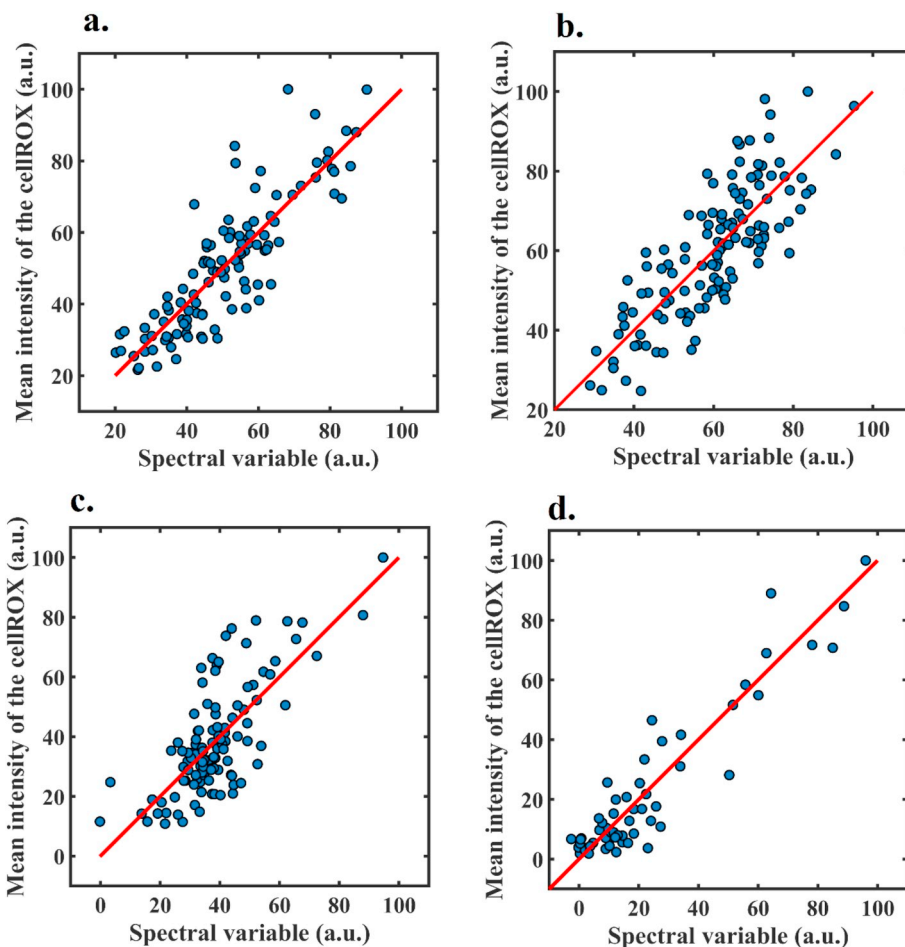
Fig. 2. Regression curve used to calibrate the AFMI system to measure the states of the ROS using full spectrum. (a) HeLa (R = 0.86), (b) PANC1 (R = 0.83), (c) MSC (R = 0.76) (d) kidney tissue (R = 0.92).
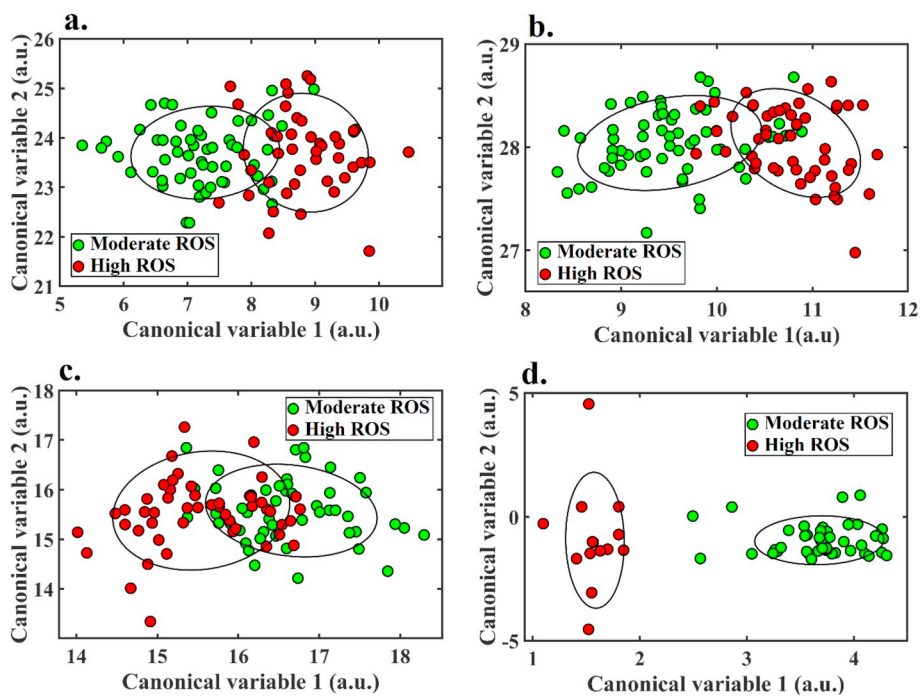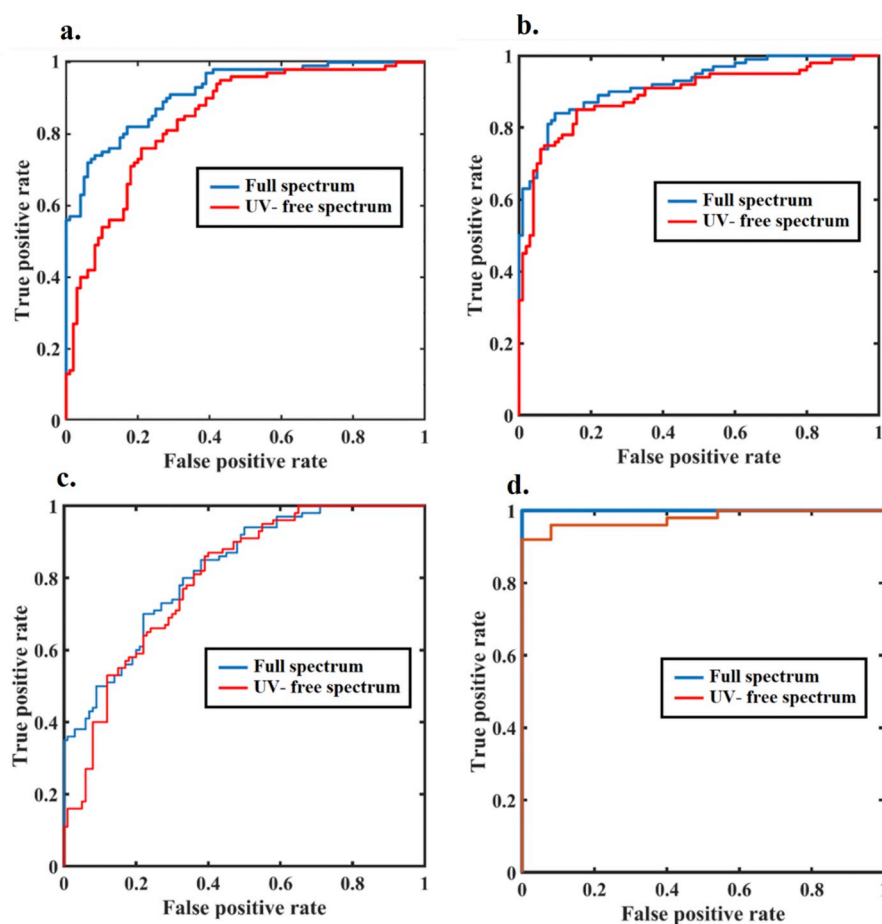

Fig. 3. Cell/tissue classification into high and moderate ROS. To visualize the data distribution for each group, an ellipse was defined for each cluster which represents the standard deviation of the data points. (a) HeLa cells (IoU = 8.3%), (b) PANC1 cells (IoU = 5.1%), (c) MSCs (IoU = 22%) (d) kidney tissue (IoU = 0%). Results shown here used the full-spectral range.

Fig. 4. ROC curve for the accuracy of discrimination between cells and tissues with different level of ROS (a) HeLa cells (AUC = 0.92/0.84 and Sensitivity = 91%/81% for full spectrum/UV- free spectrum), (b) PANC1 cells (AUC = 0.92/0.89, Sensitivity = 90%/87%), (c) MSCs (AUC = 0.82/0.80, Sensitivity = 75%/70%) (d) CKD tissue (AUC = 1.00/0.98, Sensitivity = 100%/95%).

and tissues. We developed calibration curves and classifiers for automatic measurement. AFMI provides a promising measurement tool for ROS which can be translated to future clinical and research applications.

Declaration of competing interest

Authors declare no conflict of interest.

Appendix A. Supplementary data

Supplementary data to this article can be found online at https://doi.org/10.1016/j.redox.2020.101561.

References

[1] L.A. del Rio, ROS and RNS in plant physiology: an overview, J. Exp. Bot. 66 (10) (2015) 2827–2837.
[2] V.J. Thannickal, B.L. Fanburg, M. Physiology, Reactive oxygen species in cell signaling, Am. J. Physiol. Lung Cell Mol. Physiol. 279 (6) (2000) L1005–L1028.
[3] T. Finkel, Signal transduction by reactive oxygen species, J. Cell Biol. 194 (1) (2011) 7–15.
[4] K. Abe, et al., In vivo imaging of reactive oxygen species in mouse brain by using [3H] hydromethidine as a potential radical trapping radiotracer, 34 (12) (2014) 1907–1913.
[5] L. Wu, et al., Reaction-based fluorescent probes for the detection and imaging of reactive oxygen, nitrogen, and sulfur species, 52 (9) (2019) 2582–2597.
[6] W.J.P.r. Droge, Free radicals in the physiological control of cell function, 82 (1) (2002) 47–95.
[7] U.S. Srinivas, et al., ROS and the DNA Damage Response in Cancer, (2018), p. 101084.
[8] B. Kalyanaraman, et al., Measuring reactive oxygen and nitrogen species with fluorescent probes: challenges and limitations, 52 (1) (2012) 1–6.
[9] B. D'Autréaux, M.B. Toledano, ROS as signalling molecules: mechanisms that generate specificity in ROS homeostasis, Nat. Rev. Mol. Cell Biol. 8 (10) (2007) 813.
[10] R. Datta, et al., Fluorescence Lifetime Imaging of Endogenous Biomarker of Oxidative Stress vol. 5, (2015), p. 9848.
[11] A.J. Payne, et al., Antioxidant drug therapy approaches for neuroprotection in chronic diseases of the retina, 15 (2) (2014) 1865–1886.
[12] C. Sun, et al., A reactive oxygen species scoring system predicts cisplatin sensitivity and prognosis in ovarian cancer patients, 19 (1) (2019) 1061.
[13] P. Cheng, et al., Near-infrared fluorescence probes to detect reactive oxygen species for keloid diagnosis, 9 (30) (2018) 6340–6347.
[14] J. Huang, et al., Molecular Optical Imaging Probes for Early Diagnosis of Drug-Induced Acute Kidney Injury, (2019), pp. 1–11.
[15] Y. Luo, et al., Measurement of reactive oxygen species by fluorescent probes in pancreatic cancer cells, Pancreatic Cancer, Springer, 2019, pp. 207–219.
[16] M.C. Prunty, et al., In vivo imaging of retinal oxidative stress using a reactive oxygen species–activated fluorescent probe, 56 (10) (2015) 5862–5870.
[17] R. Sharma, et al., Methods to measure reactive oxygen species (ROS) and total antioxidant capacity (TAC) in the reproductive system, Oxidative Stress in Human Reproduction, Springer, 2017, pp. 17–46.
[18] J. Woolley, J. Stanicka, T.G. Cotter, Recent advances in reactive oxygen species measurement in biological systems, Trends. Biochem. Sci. 38 (11) (2013) 556–565.
[19] C. Xie, et al., Nanoparticle regrowth enhances photoacoustic signals of semi-conducting macromolecular probe for in vivo imaging, 29 (44) (2017) 1703693.
[20] A. Habibalahi, et al., Optimized autofluorescence spectral signature for non-invasive diagnostics of ocular surface squamous neoplasia, OSSN 7 (2019) 141343–141351.
[21] A. Habibalahi, et al., Novel Automated Non Invasive Detection of Ocular Surface Squamous Neoplasia Using Multispectral Autofluorescence Imaging, (2019).
[22] M.E. Gosnell, et al., Functional hyperspectral imaging captures subtle details of cell metabolism in olfactory neurosphere cells, disease-specific models of neurodegenerative disorders, Biochim. Biophys. Acta Mol. Cell Res. 1863 (1) (2016) 56–63 %@

0167-4889.

[23] M.J. Bertoldo, et al., NAD+ repletion rescues female fertility during, Reproductive Aging 30 (6) (2020) 1670–1681 e7.

[24] P. Bondza-Kibangou, et al., Modifications of cellular autofluorescence emission spectra under oxidative stress induced by 1 α, 25dihydroxyvitamin D3 and its analog EB1089, 3 (4) (2004) 383–391.

[25] P. Bondza-Kibangou, et al., Microspectrofluorometry of autofluorescence emission from human leukemic living cells under oxidative stress, 93 (5) (2001) 273–280.

[26] G.A. Wagnieres, W.M. Star, B.C. Wilson, In vivo fluorescence spectroscopy and imaging for oncological applications, Photochem. Photobiol. 68 (5) (1998) 603–632 %@ 1751-1097.

[27] S. Isenmann, et al., TWIST family of basic helix-loop-helix transcription factors mediate human mesenchymal stem cell growth and commitment, Stem Cell. 27 (10) (2009) 2457–2468.

[28] S. Shi, S. Gronthos, Perivascular niche of postnatal mesenchymal stem cells in human bone marrow and dental pulp, J. Bone Miner. Res. 18 (4) (2003) 696–704.

[29] S. Sukjamnong, et al., MitoQ supplementation prevent long-term impact of maternal smoking on renal development, oxidative stress and mitochondrial density in male mice offspring, 8 (1) (2018) 6631.

[30] M.E. Gosnell, et al., Quantitative non-invasive cell characterisation and discrimination based on multispectral autofluorescence features, Sci. Rep. 6 (2016) 23453 %@ 2045-2322.

[31] A.U. Rehman, et al., Fluorescence quenching of free and bound NADH in HeLa cells determined by hyperspectral imaging and unmixing of cell autofluorescence, Biomed. Optic Express 8 (3) (2017) 1488–1498 %@ 2156-7085.

[32] M. Gosnel, Unlocking the Potential of Spectral Imaging for the Characterization of Cells and Stem Cells Population, Macquarei University, Thesis, 2013.

[33] S.B. Mahbub, et al., Statistically strong label-free quantitative identification of native fluorophores in a biological sample, Sci. Rep. 7 (1) (2017) 15792 %@ 2045-2322.

[34] E.C.C. Celeghini, et al., Efficiency of CellROX Deep Red® and CellROX Orange® Fluorescent Probes in Identifying Reactive Oxygen Species in Sperm Samples from High and Low Fertility Bulls, (2019), pp. 1–7.

[35] Panigrahi, B.K., Y. Shi, and M.-H. Lim, Handbook of Swarm Intelligence: Concepts, Principles and Applications. Vol. vol. 8 %@ 364217390X. 2011: Springer Science & Business Media.

[36] A. Habibalahi, M.J.M.S. Safizadeh, Technology, Pulsed eddy current and ultrasonic data fusion applied to stress measurement, 25 (5) (2014) 055601.

[37] A. Habibalahi, M.S. Safizadeh, Monitoring, *Forward to residual stress measurement by using pulsed eddy current technique*, Insight - Non-Destructive Testing and Condition Monitoring 55 (9) (2013) 492–497.

[38] V. Vapnik, The Nature of Statistical Learning Theory, Springer science & business media, 2013.

[39] A. Shrivastava, V.B. Gupta, Methods for the determination of limit of detection and limit of quantitation of the analytical methods, Chronicles Young Sci. 2 (1) (2011) 21.

[40] K. Yamada, et al., The simultaneous measurement of nicotinamide adenine dinucleotide and related compounds by liquid chromatography/electrospray ionization tandem mass spectrometry, 352 (2) (2006) 282–285.

[41] D. Williamson, P. Lund, H.J.B.J. Krebs, The redox state of free nicotinamide-adenine dinucleotide in the cytoplasm and mitochondria of rat liver, 103 (2) (1967) 514.

[42] A. Habibalahi, et al., Improving pulse eddy current and ultrasonic testing stress measurement accuracy using neural network data fusion, 9 (4) (2015) 514–521.

[43] D.J. Hand, R.J. Till, A simple generalisation of the area under the ROC curve for multiple class classification problems, Mach. Learn. 45 (2) (2001) 171–186 %@ 0885-6125.

[44] C. Cabello-Verrugio, et al., Oxidative Stress in Disease and Aging: Mechanisms and Therapies, (2016) 2016.

[45] A. Umeno, V. Biju, Y.J.F.r.r. Yoshida, In vivo ROS production and use of oxidative stress-derived biomarkers to detect the onset of diseases such as Alzheimer's disease, Parkinson's disease, and diabetes 51 (4) (2017) 413–427.

[46] F. Giacco, M.J.C.r. Brownlee, Oxidative stress and diabetic complications, 107 (9) (2010) 1058–1070.

[47] R.A. Kowluru, P.-S. Chan, Oxidative Stress and Diabetic Retinopathy, Exp. Diabetes Res. 2007 (2007) .